NASA TECHNICAL MEMORANDUM

NASA TM X-3134

NASA TM X-3134

PREDICTION OF AXIAL-FLOW INSTABILITIES IN A TURBOJET ENGINE BY USE OF A MULTISTAGE COMPRESSOR SIMULATION ON THE DIGITAL COMPUTER

Carl J. Daniele, Ronald J. Blaha, and Kurt Seldner

Lewis Research Center
Cleveland, Ohio 44135

NATIONAL AERONAUTICS AND SPACE ADMINISTRATION • WASHINGTON, D. C. • JANUARY 1975

1. Report No. NASA TM X-3134	2. Government Accession No.	3. Recipient's Catalog No.
4. Title and Subtitle PREDICTION OF AXIAL-FLOW INSTABILITIES IN A TURBOJET ENGINE BY USE OF A MULTISTAGE COMPRESSOR SIMULATION ON THE DIGITAL COMPUTER		5. Report Date January 1975 6. Performing Organization Code
7. Author(s) Carl J. Daniele, Ronald J. Blaha, and Kurt Seldner		8. Performing Organization Report No. E-8008 10. Work Unit No. 501-24
9. Performing Organization Name and Address Lewis Research Center National Aeronautics and Space Administration Cleveland, Ohio 44135		11. Contract or Grant No. 13. Type of Report and Period Covered Technical Memorandum
12. Sponsoring Agency Name and Address National Aeronautics and Space Administration Washington, D.C. 20546		14. Sponsoring Agency Code

15. Supplementary Notes

16. Abstract

A method of estimating the undistorted stall line for an axial-flow compressor by using the digital computer is presented. The method involves linearization of nonlinear dynamic equations about an operating point on a speed line, and then application of the first method of Lyapunov to determine the stability of the nonlinear system from the stability of the linear system. The method is applied to a simulation of the J85 compressor, which utilizes stage stacking and lumped volume techniques for the interstage regions to simulate steady-state and dynamic compressor performance. The stability boundary predicted by the digital simulation compares quite well with the stall line predicted by a dynamic simulation of the J85 compressor programmed on the analog computer. Since previous studies have shown that the analog-predicted stall line agrees well with the stall line of the compressor, the digital method presented is also a good means of estimating the stall line.

17. Key Words (Suggested by Author(s))	18. Distribution Statement
Compressor stability Eigenvalue analyses	Unclassified - unlimited STAR Category 28

19. Security Classif. (of this report)	20. Security Classif. (of this page)	21. No. of Pages	22. Price*
Unclassified	Unclassified	35	$3.25

* For sale by the National Technical Information Service, Springfield, Virginia 22151

PREDICTION OF AXIAL-FLOW INSTABILITIES IN A TURBOJET ENGINE BY USE OF A MULTISTAGE COMPRESSOR SIMULATION ON THE DIGITAL COMPUTER

by Carl J. Daniele, Ronald J. Blaha, and Kurt Seldner

Lewis Research Center

SUMMARY

A method of estimating the undistorted stall line for an axial-flow compressor by using the digital computer is presented. The method involves linearization of nonlinear dynamic equations (state equations) about an operating point on a speed line. The linearization process is accomplished by using finite differences. (Each state variable is incremented in turn while all others are held constant. The resulting change in the state equations is calculated.) The changes in the state equations are divided by the change in the state variable to give the first partial derivative. These first partial derivatives form a linear system matrix. Then the first method of Lyapunov is applied to determine the stability of the nonlinear system from the stability of the linear system. The method is applied to a simulation of the J85 compressor which utilizes stage stacking and lumped volume techniques for the interstage regions to simulate steady-state and dynamic compressor performance. The stability boundary predicted by the digital simulation compares quite well with the stall line predicted by a dynamic simulation of the J85 compressor programmed on the analog computer. The method of stall prediction on the analog computer is to proceed up a compressor speed line until a small amplitude limit cycle is observed. Since previous studies have shown that the analog-predicted stall line agrees well with the experimental stall line of the compressor, the digital method presented is also a good means of estimating the stall line.

INTRODUCTION

The steady-state and transient performance of airplane propulsion systems using axial-flow compressors is greatly affected by the compressor-stall characteristics. Compressor stall adversely affects engine performance and engine life and can cause inlet unstarts in supersonic aircraft. Thus, the need for determining the stall line for these compressors is evident.

Until recently stall lines for axial-flow compressors could only be determined experimentally. However, engine experiments to define stall lines are costly and time consuming. Thus, there is a need to determine these stall lines analytically. In reference 1 it is shown that an analog simulation can accurately predict the undistorted stall line for the J85 turbojet engine. However, the ability to predict stall depends on the stage characteristics of the compressor that must be determined experimentally. The eight-stage axial compressor was modeled on the analog computer by using stage performance maps and a volume behind each stage to simulate gas dynamics (lumped volume). Also included in the simulation was a burner volume followed by a choked nozzle (simulating a choked turbine nozzle).

The procedure to define stall on the analog computer is to start at a steady-state operating point on a speed line and to slowly decrease nozzle area. This causes an increase of back pressure on the compressor so that the operating point moves up the speed line. At some point a limit cycle is observed, which increases in amplitude as the operating point continues up the speed line. The compressor stall point on that speed line is assumed to be the point at which the limit cycle is first observed.

A digital simulation of the J85 engine was also formulated. The compressor was modeled on the digital computer in the same way it was modeled on the analog. The digital simulation transient analysis proved to be too time consumming because of the serial and discrete (rather than parallel and continuous) nature of the digital computer. To simulate dynamics correctly, the time step used must be smaller than the smallest time constant in the system, which necessitated a time step of 50 microseconds for the J85 simulation. In addition, small amplitude limit cycles are difficult to detect and distinguish from numerical instability, which may be induced by the numerical integration process.

Therefore, a new method for determining the stall line from the digital simulation was developed and is the subject of this report. The method involves lineariza-

tion of the nonlinear system of equations (state equations) that defines the compressor simulation about a steady-state operating point, thereby obtaining a linear system matrix. The elements of the system matrix are the partial derivatives of the state equations with respect to the state variables. The linearization of the nonlinear equations and the calculation of matrix elements is accomplished by finite differences. The eigenvalues of the system matrix are the poles of the system. If the poles all have negative real parts (in the left half plane in Laplace space), the system is stable. However, if one or more eigenvalues has a positive real part, the system is unstable. The stall point on the speed line is assumed to be the point at which positive eigenvalues are encountered. This method for determining the stability of the nonlinear system from the stability of the linear system is based on the first method of Lyapunov. The procedure is readily mechanized on the digital computer and requires very little computer time because there is no integration of dynamic variables.

The report is arranged in the following manner: First a short description of the J85 engine is given. Then a complete description of the steady-state and dynamic equations used to model the compressor is given. The steady-state equations are used to obtain an operating point on a speed line. Next, the methods of implementing the compressor model on analog and digital computers and the methods of stall prediction from each simulation are described. The stall lines predicted by both simulations are compared. Also compared are the frequency responses of the two methods. After this an eigenvector analysis of unstable modes of the linearized system is presented. Finally, an approximation is made to simplify the compressor representation and thus reduce the number of state equations. This results in a smaller system matrix. The stall line prediction of this simplified model is compared to the full variable model.

ENGINE DESCRIPTION

The analysis in this report is applied to the J85-13 afterburning turbojet engine. The engine consists of an eight-stage, axial-flow compressor, a two-stage turbine, variable inlet and outlet guide vanes, controlled interstage bleeds, and variable exhaust nozzle. The inlet guide vanes are scheduled as a function of corrected speed; the outlet guide vanes are fixed, but the pressure drop across them varies

with corrected weight flow. The interstage bleeds are on the third, fourth, and fifth compressor stages and are also scheduled as a function of corrected speed. (The bleeds are closed above 95.5 percent corrected speed, are full open at 80 percent speed, and below, and vary with speed in between.) A simulation of the whole engine is described in reference 2.

SIMULATION MODEL

The multistage compressor portion of the analog and digital simulations uses steady-state stage characteristics and an associated stage volume for gas dynamics to represent individual stages. Each compressor stage is modeled with pressure and temperature maps; each volume, with lumped continuity, energy, and momentum equations. The inlet and outlet guide vanes are modeled as pressure drops into and out of the first and last stages, respectively - the amount of pressure drop being a function of corrected speed on the digital and corrected weight flow on the analog. Bleed flows are included for the third, fourth, and fifth stages; the amount of bleed flow is also a function of corrected speed. In both analog and digital simulations, the bleeds are assumed choked. Between the last compressor stage and turbine, a burner volume is modeled. No heat addition is included, however, because only the compressor, rather than the whole engine, is of interest for this report. Behind the burner a choked nozzle is used to terminate the simulation. The choked nozzle simulates a choked turbine in the actual engine. A schematic of an ideal compressor stage is shown in figure 1. All symbols are defined in appendix A. The steady-state representation of the compressor stage is presented in appendix B, and the equations for the lumped volume gas dynamics are given in appendix C.

Steady-State Equations

The steady-state performance of the axial-flow compressor is calculated by using the stage stacking technique described in reference 1. In this technique the discharge conditions of one stage are used as the inlet conditions to the next stage. The steady-state performance for each stage is given by pressure and temperature rise coefficients ψ_c^P and ψ_c^T. These coefficients are defined (in appendix B) as

$$\psi^{P}_{c,\,n} = \frac{C_n T_{tv,\,n-1}}{N^2}\left[\left(\frac{P_{tc,\,n}}{P_{tv,\,n-1}}\right)^{2/7} - 1\right] \tag{1}$$

$$\psi^{T}_{c,\,n} = \frac{C_n}{N^2}\,(T_{tc,\,n} - T_{tv,\,n-1}) \tag{2}$$

Representative maps of ψ^P and ψ^T as a function of flow coefficient Φ are shown in figures 2 and 3, respectively. The flow coefficient is defined as

$$\Phi_{c,\,n} = \frac{K_n}{N}\,v_{zc,\,n} \tag{3}$$

The axial-flow velocity $v_{zc,n}$ is related to the stage-inlet total pressure and temperature (as developed in appendix B) by

$$\frac{\dot{W}_{c,\,n}\sqrt{\theta_{v,\,n-1}}}{\delta_{v,\,n-1}\mathcal{A}_{c,\,n}} = \frac{v_{zc,\,n}}{\sqrt{\theta_{v,\,n-1}}}\left[1 - \left(\frac{v_{zc,\,n}}{\sqrt{\theta_{v,\,n-1}}}\right)^2 \frac{1}{2gJC_pT_{tr}\cos^2\beta_n}\right]^{5/2} \rho_{tr} \tag{4}$$

where δ and θ are corrected pressure and temperature parameters, and β is the angle between the air velocity and the axial direction. In steady state the inlet and outlet guide vanes are modeled as pressure drops, thus

$$P_{v,\,0} = P2\,(\text{IGV PR}) - 0.005\,P2 \tag{5}$$

$$P_{OGV} = P_{tv,\,8}\,(\text{OGV PR}) \tag{6}$$

The steady-state performance of the burner volume is modeled by assuming that the pressure, temperature, and weight flow into and out of the volume are the same:

$$T_{tv,\,9} = T_{tc,\,9} \tag{7}$$

$$P_{tv,\,9} = P_{tc,\,9} \tag{8}$$

while

$$P_{tc,\,9} = P_{OGV} - K'(\dot{W}_{c,9})^2 \tag{9}$$

where K' is determined from experimental data. The nozzle area and bleed flows are assumed choked, with the amount of bleed flow area a function of corrected speed. The choked flow equation used is

$$\dot{W} = KCHOK\,\mathscr{A}\,\frac{P_t}{\sqrt{T_t}} \tag{10}$$

The steady-state equations are used to determine an operating point on a speed line.

Dynamic Equations

Compressor dynamics are simulated by using a lumped volume for each stage. Each lumped volume is located just downstream of the stage's active element. The volume dynamics are modeled through the application of continuity, energy, and momentum equations as shown in appendix C. The equations are

$$\frac{d}{dt}\,(\rho_{sv,\,n}) = \frac{1}{V_n}\,(\dot{W}_{c,\,n} - \dot{W}_{c,\,n+1}) \tag{11}$$

$$\frac{d}{dt}\,(\rho_{sv,\,n}\,T_{tv,\,n}) = \frac{\gamma}{V_n}\left[T_{tc,\,n}\,\dot{W}_{c,\,n} - T_{tv,\,n}\,(\dot{W}_{c,\,n+1} + \dot{W}_{b,\,n})\right] \tag{12}$$

and

$$\frac{d}{dt}\,(\dot{W}_{c,\,n}) = \frac{\mathscr{A}_n g}{L_n}\,(P_{tc,\,n} - P_{tv,\,n}) \tag{13}$$

While the equation of state for the gas in the volume is

$$P_{tv,\,n} = R\rho_{sv,\,n}\,T_{tv,\,n} \tag{14}$$

No dynamic effects are modeled for the inlet and outlet guide vanes, interstage bleeds, or choked nozzle. A lumped volume is included in the burner but without

an energy equation. Instead, equality of temperature is assumed:

$$T_{tv,\,9} = T_{tc,\,9} = T_{tv,\,8} \tag{15}$$

Analog Implementation of Equations

Equations (1) to (15) form a complete mathematical representation of the dynamic and steady-state characteristics of the compressor model. These equations are programmed on the analog computer. All functional relationships for steady-state stage characteristic pressures and temperatures and for bleed flows and guide vanes are generated by using diode function generators. Dynamics on the analog computer are calculated by integrating the dynamic equations (11) to (13). The temperatures in the stage volumes are calculated by integrating equations (11) and (12) to obtain ρ and ρT, respectively.

The method of stall prediction on the analog simulation is to start with a steady-state operating point on a speed line. The nozzle area is then slowly decreased so that back pressure on the compressor is slowly increased. This causes the operating point to move slowly up the speed line. At some point a small amplitude limit cycle is observed. Further movement up the speed line results in an increase in amplitude of the limit cycle. The stall point for the speed line is assumed to be the point at which the limit cycle is first observed. By repeating this procedure for a number of speed lines, the undistorted stall line is defined.

Digital Implementation of Equations

The equations could also be programmed into the digital computer. It would be possible to determine the stall line for the compressor on the digital computer in the same way it was done on the analog simulation. Digital simulation of a dynamic system with small time constants necessitates a time step smaller than the smallest time constant in the system. This results in large amounts of computer time to obtain a transient solution. In addition, small amplitude limit cycles generated on a digital simulation are difficult to detect and distinguish from numerical instability induced by the integration method. The same steady-state and dynamic equations used on

the analog computer are also used on the digital computer to describe the system. However, on the digital computer, the dynamic equations are not integrated, and no transient solution is obtained.

STABILITY ANALYSIS

Consider the system of nonlinear differential equations:

$$\dot{X} = f(X, u^*) \tag{16}$$

where X and f are ℓ-vectors (ℓ equals 26 for this problem) and u^* is an m-vector of inputs. One way to determine the stability of this nonlinear system is the method of Lyapunov, as presented in reference 3. Let the steady-state solution of this system of equations be given by $X = X_o$, so that $f(X_o, u_o^*) = 0$. This system can be linearized and the steady-state operating point translated to the origin; the resulting equations are given by

$$\dot{Y} = AY + Bu \tag{17}$$

where

$$\left.\begin{aligned} Y &= X - X_o \\ u &= u^* - u_o^* \end{aligned}\right\} \tag{18}$$

A is the Jacobian matrix, such that

$$A_{ij} = \frac{\partial f_i}{\partial X_j} \qquad \begin{matrix} i = 1, \ \ell \\ j = 1, \ \ell \end{matrix} \tag{19}$$

and B is an ℓ by m matrix, such that

$$B_{ij} = \frac{\partial f_i}{\partial u_j} \qquad \begin{matrix} i = 1, \ \ell \\ j = 1, \ m \end{matrix} \tag{20}$$

For the free dynamic system $\dot{Y} = AY$, Lyapunov showed that, if the eigenvalues λ of A have nonzero real parts, then the stability of the operating point X_o for the nonlinear system is the same as that of the operating point $Y = 0$ for the linearizied system. The eigenvalues are the roots of the characteristic equation for the linearizied system and are determined by

$$|A - \lambda I| = 0 \tag{21}$$

If all the eigenvalues have negative real parts (lie in the left half plane in Laplace space), the linear system is stable, and hence the nonlinear system is stable in a region about the operating point. If at least one eigenvalue has a positive real part, the nonlinear system is unstable.

The first method of Lyapunov is applied to the compressor simulation already described. An operating point is chosen on a speed line and the steady-state values for the state variables are determined. The 26 state equations are linearized about the operating point, and the system matrix A of first partial derivatives is generated. This is accomplished by using finite differences. Each state variable is varied in turn, while the others are held constant. If each state variable is changed by d_j, then:

$$\frac{\partial}{\partial X_j}\left(\frac{d}{dt} X_i\right) \approx \frac{f_i\left|X_j + d_j\right. - \cancel{f_i\left|X_j\right.}}{X_j + d_j - X_j} \qquad \text{(0 (zero in steady state))} \tag{22}$$

The eigenvalues of A are calculated by use of digital programs presented in reference 4. If all the eigenvalues have negative real parts, the system is stable at that operating point. (The compressor is not in stall.) A point is chosen farther up the speed line, and the same procedure is performed. This process is continued until at least one eigenvalue has a positive real part (in the right half plane in Laplace space). At this point the compressor is assumed to be in stall, and the stall point on the speed line is assumed to be the point just before the positive eigenvalue is encountered.

A comparison of analog and digital stability assumptions is of interest. For the analog simulation stall is assumed to occur when a limit cycle is observed. For

the digital simulation stall is assumed to occur when positive eigenvalues are encountered. It can be shown rather easily and is implied by the Lyapunov theory that, if the linear system is stable, the states converge to their steady-state values for the nonlinear system. Thus, if all the eigenvalues of the linear system have negative real parts, there can be no limit cycle for the nonlinear system. However, if the linear system is unstable, the states of the nonlinear system may diverge or may have a limit cycle.

RESULTS

Stall Line

The comparison of stall points generated by the analog and digital J85 compressor simulations is shown in figure 4. Ten corrected speed lines are shown. The speed lines shown were obtained on the analog computer. (Speed lines obtained on the digital computer were nearly identical.) The analog generated and digital generated stall points shown in figure 4 are quite close. The slight error in the 85 and 87 percent speed lines can be attributed to the difficulty in defining the exact point where a limit cycle started with the analog simulation. The results in figure 4 are for sea-level-static inlet conditions. However, since no Reynolds number effects are included in the simulation, the results apply only for high Reynolds number conditions. The results show that the digital-state variable analysis can duplicate analog results. The analog method of determining the undistorted stall line has already been verified. Thus, the digital state variable analysis is also a good means of determining the undistorted stall line for axial-flow compressors.

Figure 5 shows a pseudo-root locus for the digital compressor representation. It shows the motion of eigenvalues through Laplace space as the operating point approached stall on the 100-percent speed line. This is not a conventional root locus since the whole system is essentially redefined at each point as the operating point moves up the speed line. The figure shows only the upper half plane since the lower half is the mirror image. The log scale is used since large decade changes occurred in the eigenvalues that did move significantly. However, since there is no zero on a log scale, the eigenvalues must be assumed to go through zero somewhere between the values -0.001 and +0.001 on the abscissa. The circle data

symbols indicate that very little change in the eigenvalue position occurred as the operating point changed. The five operating points shown started just before stall (points 1 to 3) where point 3 is the stall point given in figure 4. Operating point 4 is just into stall and operating point 5 is farther into stall. The decrease in weight flow from one operating point to the next was 0.045 kilogram per second. Note that for the speed line shown four eigenvalues (two shown plus their complex pairs) crossed the imaginary axis almost simultaneously. To determine which pair crossed first, a smaller weight flow step would have to be taken; however, this was not done because a tolerance of 0.045 kilogram per second is within experimental accuracy. The fifth operating point is shown because it indicates that further movement up the speed line caused those eigenvalues already in the right half plane to move farther to the right and another eigenvalue to move closer to becoming unstable.

Frequency Response

The frequency responses generated by the analog and digital simulations were also compared. The two inputs available for the frequency response were P2, the input pressure and $\mathcal{A}_{10}$, the nozzle area. The analog response was measured by using a discrete frequency analyzer with the simulation. The digital response was calculated by taking the Laplace transform of equations (17). Matrix B was calculated by keeping all the state variables constant and perturbing each input separately while keeping the other constant. The resulting change in Y was calculated and the B matrix determined as

$$B = \begin{bmatrix} \frac{\Delta \dot{Y}_1}{\Delta u_1} & \frac{\Delta \dot{Y}_1}{\Delta u_2} \\ \frac{\Delta \dot{Y}_2}{\Delta u_1} & \frac{\Delta \dot{Y}_2}{\Delta u_2} \\ \vdots & \vdots \\ \frac{\Delta \dot{Y}_{26}}{\Delta u_1} & \frac{\Delta \dot{Y}_{26}}{\Delta u_2} \end{bmatrix} \tag{23}$$

This procedure was accomplished on the digital computer by using finite differences. Then, using matrices A and B the frequency response was calculated using the digital programs found in reference 5. A comparison of frequency responses of the analog and digital compressor simulations is shown in figures 6. The operating point chosen for the frequency responses was on the 100-percent speed line at a weight flow of 19.739 kilograms per second and a pressure ratio of 6.79. Three frequency responses are shown - $P_{v,1}/P2$, $\dot{W}_{c,1}/P2$, and $P_{OGV}/\mathscr{A}_{10}$. In all cases there was good agreement up to about 20 hertz, at which point the two responses started to diverge. The reason for the discrepancy, however, is not clear since both simulations contained the same volume dynamics.

Eigenvector Analysis

Digital programs from reference 4 also have the capability of determining the eigenvectors associated with the eigenvalues. The eigenvectors are defined by

$$Ae_i = \lambda e_i \tag{24}$$

where eigenvector e_i is a nonzero vector and is associated with eigenvalue λ_i. From reference 3, if λ_i is real, the motion $e^{\lambda_i t}$ is along the eigenvector e_i. If λ_i is greater than zero, then $e^{\lambda_i t}$ along e_i approaches infinity; if less than zero, it approaches the origin of the state. If λ_i is complex, the combined motion of it and its complex conjugate is oscillatory and takes place in the plane determined by their associated eigenvectors. If the real part of the complex eigenvalue is negative, the oscillation is damped; if positive, the oscillation goes unstable.

The eigenvectors were calculated for the operating point just beyond stall, where at least one eigenvalue had a positive real part. For each eigenvalue there was a corresponding eigenvector (26 for this system). Each eigenvector had 26 components - the first component being related to the first state variable and so on. Since the eigenvectors represent the fundamental modes of the system, the state variables ρ and ρT were changed to pressure and temperature, using equations (11), (12), and (14), to relate the results to more physically understandable quantities. For all 10 speed lines, the eigenvalues that were unstable were complex; thus, there were two eigenvectors associated with the instability. The magnitudes of the

components of the unstable eigenvectors were calculated and divided by the magnitude of the largest component of each quantity, respectively. (All pressures changes were divided by the largest pressure change; all weight flow changes by the largest weight flow change; and all temperature changes by the largest temperature change.) This nondimensionalized the numbers so that they could be compared. The resulting modal maps for the 100-percent speed line are shown in figure 7. For this speed line the values given are for the unstable eigenvalue at an imaginary value of 11 000 radians per second in figure 5. Note from figure 7 that the largest relative motion in pressure occurred in the eighth stage, weight flow in the third stage, and temperature in the second stage. Although the phase is not shown, pressure and weight flow motions are 90° out of phase with weight flow leading pressure. Temperature motion is in phase with pressure. Also, for any two successive stages, vectors of like quantities could be 180° out of phase. It is impossible to state which stage caused stall since the eigenvectors are really a composite of the total motion in the system.

No conclusions could be drawn from these results, as the significance of this method has not been fully investigated. Different state variables or a closer look at actual stage pressure and temperature ratios may give more definitive results.

Modified Simulation

The digital simulation consists of three state variables per stage. However, if it is desired to predict the loss in performance and surge margin due to distorted inlet flow, circumferential or radial effects would have to be included in addition to axial flow, and the number of state variables could increase drastically. Alternatively, it may be desired to determine the undistorted stall line for a more complex engine (such as a two spool turbofan), which would also cause a large increase in the number of state equations. In anticipation of such problems, a simplification of the volume dynamics was made by arbitrarily eliminating the temperature dynamics in the compressor stages:

$$T_{tv,\,n} = T_{tc,\,n} \tag{25}$$

Using equation (25) and combining equations (12) and (14) result in

$$\frac{d}{dt}(P_{tv,n}) = \frac{\gamma R T_{tv,n}}{V_n}(\dot{W}_{c,n} - \dot{W}_{c,n+1} - \dot{W}_{b,n}) \tag{26}$$

$$\frac{d}{dt}(\dot{W}_{c,n}) = \frac{\mathscr{A}_n g}{L_n}(P_{tc,n} - P_{tv,n}) \tag{13}$$

From equations (13), (25), and (26), the modified digital simulation consisted of 18 state variables - two for each compressor stage and two for the burner volume. Here also a choked nozzle was used to terminate the burner volume.

Figure 8 shows the comparison of stall points generated by the unmodified digital and modified digital simulations. The same speed lines are shown as in figure 4. From figure 8 the results compare quite well for the lower speed lines (80 percent and below), but the results diverge at the higher speeds. This would indicate that the temperature dynamics tend to stabilize the system, the effect being most pronounced at the higher speeds. For comparison the analog simulation was also modified to eliminate the temperature dynamics. Figure 9 represents a comparison of the stall points for the same speed lines using both modified simulations. The results show good comparison between the two simulations except at 70 percent speed.

One final method of looking at the effect of the temperature dynamics is shown in figure 10. In this figure is a comparison of the eigenvalue position for the modified and unmodified digital compressor simulations just after the stall limit for the modified simulation. At the same operating point on the 100-percent speed line, all the eigenvalues for the unmodified simulation are to the left of those for the modified simulation. Because this figure is in Laplace space, a more stable system for the unmodified simulation is indicated. From figure 10 each modified eigenvalue corresponds to an eigenvalue from the unmodified system. The modified eigenvalue, which is unstable, has an imaginary value of 36 000 radians per second. However, from figure 5 this eigenvalue remains in about the same relative position as the operating point moves up the speed line and does not become unstable. Instead, the two eigenvalues with imaginary parts of about 11 000 and 15 000 radians per second are the ones that become unstable for the unmodified simulation, while remaining stable for the modified simulation. Finally, the modified state variable method does give

good stall-line prediction for lower speeds, but eliminating the temperature dynamics does degrade stall prediction at the higher speeds. Therefore, the use of this method in solving future problems should be considered carefully.

CONCLUSIONS

A new method of determining the undistorted stall line for an axial-flow compressor simulation using the digital computer has been presented. The simulation uses the stage stacking and lumped volume techniques first used to define the stall line by the analog computer. The method employs small changes about an operating point to form linearized state equations for the system. The stability of the nonlinear system is obtained from the stability of the linear system by the first method of Lyapunov.

This procedure was applied to an eight-stage simulation of the J85 compressor. Three state variables were assumed for each stage. The analysis was done for 10 compressor speed lines, and the stall point was defined on each. There was good agreement between the analog and digital stall-point predictions. Since the analog previously matched experimental results, the digital method presented in this report is also a good means of determining the stall lines for axial-flow compressors. Also, frequency responses from the two simulations were compared. Good agreement between the two existed up to about 20 hertz, at which point they started to diverge. Using the eigenvalues at a point just into stall, the corresponding eigenvectors were calculated. From the eigenvectors, modal maps of pressure, weight flow, and temperature were drawn. The largest relative motion in pressure occurred in the eighth stage; weight flow, in the third stage; and temperature, in the second stage. However, no conclusions could be drawn from this analysis, and further investigation is warranted.

Next, the number of state variables for the system was reduced by arbitrarily eliminating the temperature dynamics. This modified method showed good correlation with the analog for stall prediction at low speeds (80 percent and below). However, the stall point predictions diverged at the high speeds. Evidently, the temperature dynamics tended to stabilize the system, and this stabilizing effect was

more pronounced at the higher speeds. Thus, reducing the number of state variables in future work should be considered carefully.

Lewis Research Center,
National Aeronautics and Space Administration,
Cleveland, Ohio, July 25, 1974,
501-24.

APPENDIX A

SYMBOLS

A	ℓ by ℓ Jacobian matrix
$\mathscr{A}$	area, m^2; ft^2
a	speed of sound, m/sec; ft/sec
B	ℓ by m input coefficient matrix
C	coefficient, rpm^2/K^2; $rpm^2/{}^oR^2$
C_p	specific heat at constant pressure, J/(kg-K); Btu/(lbm-^{o}R)
C_v	specific heat at constant volume, J/(kg-K); Btu/(lbm-^{o}R)
d	perturbation of state variable
e	eigenvector
g	gravitational constant, 1.0 (kg-m)/($N\text{-}sec^2$); 32.17 (lbm-ft)/($lbf\text{-}sec^2$)
h	enthalpy, J/kg; Btu/lbm
I	identity matrix
IGVPR	pressure drop due to inlet guide vanes
J	mechanical equivalent of heat, 1.0 (N-m/J); 778.3 (ft-lbf/Btu)
K	coefficient, rpm-sec/m; rpm-sec/ft
K'	constant for burner volume, $(N/m^2)/(kg/sec)^2$; $(lbf/ft^2)/(lbm/sec)^2$
KCHOK	choked flow coefficient, $\left(kg\text{-}\sqrt{K}\right)/(N\text{-}sec)$; $\left(lbm\text{-}\sqrt{{}^oR}\right)/(lbf\text{-}sec)$
k	bleed flow coefficient, $\left(kg\text{-}\sqrt{K}\right)/(N\text{-}sec)$; $\left(lbm\text{-}\sqrt{{}^oR}\right)/(lbf\text{-}sec)$
L	length, m; ft
ℓ	total number of states
M	Mach number
N	rotational speed, rpm
OGVPR	pressure drop due to outlet guide vanes

P	pressure, N/m^2; lbf/ft^2
P_2	input pressure, N/m^2; lbf/ft^2
q	internal energy, J/kg; Btu/lbm
R	universal gas constant, 287 (N-m)/(kg-K); 53.3 (lbf-ft)/(lbm-^oR)
r	radius, m; ft
T	temperature, K; ^oR
t	time, sec
U	rotor speed, m/sec; ft/sec
u	m by 1 vector of system inputs translated to the operating point
u^*	m by 1 vector of system inputs
V	volume, m^3; ft^3
v	velocity, m/sec; ft/sec
$\dot{W}$	weight flow, kg/sec; lbm/sec
X	l by 1 vector of state variables
Y	l by 1 vector of state variables translated to operating point
α	coefficient, 30 (m-sec)/(m-min); 360 (in.-sec)/(ft-min)
β	rotor air inlet angle, deg
γ	ratio of specific heats
Δ	change in variable
δ	ratio of total pressure to standard atmospheric pressure
θ	ratio of total temperature to standard atmospheric temperature
λ	eigenvalue, rad/sec
ρ	weight density, kg/m^3; lbm/ft^3
Φ	flow coefficient
ψ^P	pressure coefficient
ψ^T	temperature coefficient

Subscripts:

b	variable associated with stage bleed
c	variable associated with stage characteristic
i	matrix component position
j	matrix component position
n	stage number designation
OGV	outlet guide vanes
o	steady-state operating point
r	reference state
s	static condition
t	total condition
v	variable associated with stage volume
z	axial direction
0	input to stage one
1,2,...,8	stage numbers
9	burner volume
10	nozzle exit

Superscripts:

$\dot{}$	derivative with respect to time
—	maximum value of quantity used for normalizing

APPENDIX B

STEADY-STATE COMPRESSOR REPRESENTATION

The analytical steady-state model of the compressor is based on the stage stacking technique. The derivation of the equations is taken from appendix B of reference 1 and is presented for completeness. The stage characteristics are represented by a pair of two-dimensional curves for each stage. The individual stage performance, described by a pressure coefficient ψ^P and a temperature coefficient ψ^T, is assumed to be a function of the flow coefficient Φ. The coefficients are mathematically described by

$$\left.\begin{aligned} \psi^P &= \frac{2gJ\,\Delta h_t'}{U^2} \\ \psi^T &= \frac{2gJ\,\Delta h_t}{U^2} \\ \Phi &= \frac{v_z}{U} \end{aligned}\right\} \tag{B1}$$

The ideal total enthalpy rise for the n^{th} stage can be related to the stage total-pressure ratio from

$$\Delta h'_{tc,\,n} = C_p T_{tv,\,n-1}\left[\left(\frac{P_{tc,\,n}}{P_{tv,\,n-1}}\right)^{(\gamma-1)/\gamma} - 1\right] \tag{B2}$$

The adiabatic enthalpy rise can be determined from:

$$\Delta h_{tc,\,n} = C_p\,(T_{tc,\,n} - T_{tv,\,n}) \tag{B3}$$

and the stage wheel speed U from

$$U = \frac{\pi N r}{\alpha} \tag{B4}$$

The stage inlet conditions are associated with the conditions in the preceding volume, and the variables are subscripted accordingly. The stage exit conditions are, however, associated with the stage itself. Assuming that the n^{th} compressor stage is preceded by the $n - 1$ volume, we can combine equations (B1) with equations (B2) to (B4) to form the following set of equations for the n^{th} stage (assuming $\gamma = 1.4$):

$$\left.\begin{aligned} \psi_n^P &= \frac{C_n T_{tv,\,n-1}}{N^2}\left[\left(\frac{P_{tc,\,n}}{P_{tv,\,n-1}}\right)^{2/7} - 1\right] \\ \psi_n^T &= \frac{C_n}{N^2}\left(T_{tc,\,n} - T_{tv,\,n}\right) \\ \Phi_n &= \frac{K_n}{N} v_{zc,\,n} \end{aligned}\right\} \tag{B5}$$

where

$$C_n = \frac{2gJC_p(\alpha)^2}{\pi^2 r_n^2}$$

$$K_n = \frac{\alpha}{\pi r_n}$$

The flow coefficient Φ is defined as the ratio of the axial-flow velocity to a mean rotor velocity. Introducing the square root of the stage corrected temperature into the relation for Φ given in equations (B1), the flow coefficient becomes

$$\Phi = \frac{v_z/\sqrt{\theta}}{U/\sqrt{\theta}} \tag{B6}$$

The axial velocity v_z can be computed from the flow, total pressure, and total temperature at the stage inlet. The flow and the axial velocity are related by

$$v_z = \frac{\dot{W}}{\rho_s \mathcal{A}} \tag{B7}$$

Eliminating the density from equation (B7) with a state equation of the form

$$P_s = \rho_s R T_s$$

results in

$$v_z = \frac{\dot{W} R}{\mathcal{A}} \frac{T_s}{P_s} \tag{B8}$$

or

$$v_z = \frac{\dot{W} R}{\mathcal{A}} \frac{T_t}{P_t} \left(1 + \frac{\gamma - 1}{2} M^2\right)^{1/(\gamma-1)} \tag{B9}$$

Equation (B9) can be rewritten in terms of corrected parameters as

$$\frac{v_z}{\sqrt{\theta}} \rho_{tr} = \frac{\dot{W}\sqrt{\theta}}{\mathcal{A}\delta} \left(1 + \frac{\gamma - 1}{2} M^2\right)^{1/(\gamma-1)}$$

or

$$\frac{\dot{W}\sqrt{\theta}}{\mathcal{A}\delta} = \frac{v_z}{\sqrt{\theta}} \left(1 + \frac{\gamma - 1}{2} M^2\right)^{-1/(\gamma-1)} \rho_{tr} \tag{B10}$$

It can be shown from the energy equation that

$$\frac{v^2}{a_t^2} = \frac{2JC_p}{\gamma R}\left(1 - \frac{T_s}{T_t}\right) \tag{B11}$$

or

$$\frac{T_s}{T_t} = 1 - \frac{\gamma - 1}{2}\frac{v^2}{a_t^2}$$

Thus, since

$$\frac{T_s}{T_t} = \left(1 + \frac{\gamma - 1}{2} M^2\right)^{-1} = \left(1 - \frac{\gamma - 1}{2}\frac{v^2}{a_t^2}\right) \tag{B12}$$

combining equations (B10) and (B12) results in

$$\frac{\dot{W}\sqrt{\theta}}{\mathscr{A}\delta} = \frac{v_z}{\sqrt{\theta}}\left[1 - \left(\frac{v}{\sqrt{\theta}}\right)^2 \frac{1}{2gJC_pT_{tr}}\right]^{1/(\gamma-1)} \rho_{tr} \tag{B13}$$

It should be noted that the nonsubscripted velocity v introduced into equation (B11) is the magnitude of the velocity vector and not the axial velocity component v_z. If the airflow approaches the rotor inlet angle β,

$$v_z = v \cos \beta \tag{B14}$$

and equation (B13) becomes

$$\frac{\dot{W}\sqrt{\theta}}{\mathscr{A}\delta} = \frac{v_z}{\sqrt{\theta}}\left[1 - \left(\frac{v_z}{\sqrt{\theta}}\right)^2 \frac{1}{2gJC_pT_{tr}\cos^2\beta}\right]^{1/(\gamma-1)} \rho_{tr} \tag{B15}$$

For the n^{th} stage the flow parameter Φ_n can be described by

$$\Phi_n = \frac{K_n}{\left(\frac{N}{\sqrt{\theta_{v,\,n-1}}}\right)} \frac{v_{zc,\,n}}{\sqrt{\theta_{v,\,n-1}}} \tag{B16}$$

and the corrected axial velocity $v_{zc,n}/\sqrt{\theta_{v,n-1}}$ is determined from the solutions of equations (B15) rewritten for the n^{th} stage as

$$\frac{\dot{W}_{c,\,n}\sqrt{\theta_{v,\,n-1}}}{\mathscr{A}_n \delta_{v,\,n-1}} = \frac{v_{zc,\,n}}{\sqrt{\theta_{v,\,n-1}}} \left[1 - \left(\frac{v_{zc,\,n}}{\sqrt{\theta_{v,\,n-1}}}\right)^2 \frac{1}{2gJC_pT_{tr}\cos^2\beta_n}\right]^{1/(\gamma-1)} \rho_{tr} \tag{B17}$$

where

$$\left.\begin{aligned} \delta_{v,\,n-1} &= \frac{P_{tv,\,n-1}}{P_{tr}} \\ \theta_{v,\,n-1} &= \frac{T_{tv,\,n-1}}{T_{tr}} \end{aligned}\right\} \tag{B18}$$

APPENDIX C

STAGE GAS DYNAMICS

The gas dynamics of each compressor stage is assumed to occur in an equivalent stage volume, which is conceptually located just downstream of the stage pressure and temperature-rise characteristics. The stage gas dynamics are represented by continuity, energy, and momentum balances across the volume. The equations for the gas dynamics are developed in appendix C of reference 1 and are presented here for completeness. Assuming no work is performed in the volume and that the net heat input is negligible, an energy balance can be written for the n^{th} volume as

$$V_n \frac{d}{dt} (\rho_{sv,\,n}\, q_{tv,\,n}) = h_{tc,\,n}\, \dot{W}_{c,\,n} - h_{tv,\,n}\, \dot{W}_{c,\,n+1} \tag{C1}$$

Noting that $q_t = C_v T_t$ and that $h_t = C_p T_t$, equation (C1) becomes

$$\frac{d}{dt} (\rho_{sv,\,n}\, T_{tv,\,n}) = \frac{\gamma}{V_n} (T_{tc,\,n}\, \dot{W}_{c,\,n} - T_{tv,\,n}\, \dot{W}_{c,\,n+1}) \tag{C2}$$

To determine the density of the gas in the stage volume, it is assumed that the rate of change of the static density is proportional to the net weight flow:

$$\frac{d}{dt} (\rho_{sv,\,n}) = \frac{1}{V_n} (\dot{W}_{c,\,n} - \dot{W}_{c,\,n+1}) \tag{C3}$$

The total pressure in the stage volume is calculated from the equation of state of the form

$$P_{tv,\,n} = R(1 + 0.2\, M_{v,\,n}^2)^{5/2} (\rho_{sv,\,n}\, T_{tv,\,n}) \tag{C4}$$

A momentum balance written across the stage and its associated volume is used to provide an expression for the determination of weight flow. It is assumed that flow acceleration is caused by the difference between the static compressor head rise $\Delta P_{sc,n}$ and the head rise $(P_{sv,n} - P_{sv,n-1})$ imposed by the adjacent volumes.

Neglecting convective momentum terms, this assumption yields

$$\frac{d}{dt}\left(\dot{W}_{c,\,n}\right) = \frac{\mathscr{A}_n g}{L_n}\left[\Delta P_{sc,\,n} - \left(P_{sv,\,n} - P_{sv,\,n-1}\right)\right] \tag{C5}$$

The stage inlet conditions, however, are conditions in the inlet volume and, thus, $\Delta P_{sc,n} = P_{sc,n} - P_{sv,n-1}$ and equation (C5) becomes

$$\frac{d}{dt}\left(\dot{W}_{c,\,n}\right) = \frac{\mathscr{A}_n g}{L_n}\left(P_{sc,\,n} - P_{sv,\,n}\right) \tag{C6}$$

Assuming the Mach number at the stage exit and the volume are the same, equation (C6) can be written as

$$\frac{d}{dt}\left(\dot{W}_{c,\,n}\right) = \frac{\mathscr{A}_n g}{L_n}\left(1 + 0.2\,M_{v,\,n}^2\right)^{-7/2}\left(P_{tc,\,n} - P_{tv,\,n}\right) \tag{C7}$$

Equations (C2) to (C4) and (C7) provide a representation for the gas dynamics of the n^{th} stage volume. In the computer simulation of these equations (both analog and digital simulations) the distinction between static and total pressures was dropped. This simplification resulted in neglecting the Mach number corrections in equations (C4) and (C7). The interstage Mach numbers encountered in the compressor are less than 0.5. The range of corrections in equations (C4) and (C7) are thus

$$1.0 < \left(1 + 0.2\,M^2\right)^{5/2} < 1.13$$

$$0.84 < \left(1 + 0.2\,M^2\right)^{-7/2} < 1.0$$

The worst-case error introduced by this simplification is, thus, approximately equivalent to a 15-percent change in the coefficients. With the computer formulation used, the approximation is reflected in dynamic coefficients and does not alter

steady-state results. Neglecting the Mach number corrections results in

$$\frac{1}{V_n} (\dot{W}_{c,\,n} - \dot{W}_{c,\,n+1}) = 0$$

$$\frac{\gamma}{V_n} (T_{tc,\,n}\, \dot{W}_{c,\,n} - T_{tv,\,n}\, \dot{W}_{c,\,n+1}) = 0$$

and

$$\frac{\mathcal{A}_n g}{L_n} (P_{tc,\,n} - P_{tv,\,n}) = 0$$

in the steady state. Equations (C8) thus yield

$$\left.\begin{aligned} \dot{W}_{c,\,n} &= \dot{W}_{c,\,n+1} \\ T_{tc,\,n} &= T_{tv,\,n} \\ P_{tc,\,n} &= P_{tv,\,n} \end{aligned}\right\} \tag{C9}$$

in the steady state. Thus, the steady-state results are unaffected by approximations in the volume dynamics.

Interstage bleed can be included in the compressor simulation by modifying equations (C2) and (C3). The bleed flow can be computed from the relation:

$$\dot{W}_{b,\,n} = k_b \mathcal{A}_{b,\,n} \frac{P_{tv,\,n}}{\sqrt{T_{tv,\,n}}} \tag{C10}$$

which assumes choked flow. Including the effects of interstage bleed changes equations (C2) and (C3) to

$$\frac{d}{dt}(\rho_{sv,\,n}\, T_{tv,\,n}) = \frac{\gamma}{V_n} \left[T_{tc,\,n}\, \dot{W}_{c,\,n} - T_{tv,n}\, (\dot{W}_{c,\,n+1} + \dot{W}_{b,\,n})\right] \tag{C11}$$

$$\frac{d}{dt}(\rho_{sv,\,n}) = \frac{1}{V_n} (\dot{W}_{c,\,n} - \dot{W}_{c,\,n+1} - \dot{W}_{b,\,n}) \tag{C12}$$

REFERENCES

1. Willoh, Ross G.; and Seldner, Kurt: Multistage Compressor Simulation Applied to the Prediction of Axial Flow Instabilities. NASA TM X-1880, 1969.

2. Seldner, Kurt; Mihaloew, James R.; and Blaha, Ronald J.: Generalized Simulation Technique For Turbojet Engine System Analysis. NASA TN D-6610, 1972.

3. Ogata, Katsuhiko: State Space Analysis of Control Systems. Prentice-Hall, Inc., 1967.

4. Geyser, Lucille C.; and Lehtinen, Bruce: Digital Program for Solving the Linear Stochastic Optimal Control and Estimation Problem. NASA TN D-7820, 1974.

5. Seidel, Robert C.: Computer Programs for Calculations of Matrix Stability and Frequency Response from a State-Space System Description. NASA TM X-71581, 1974.

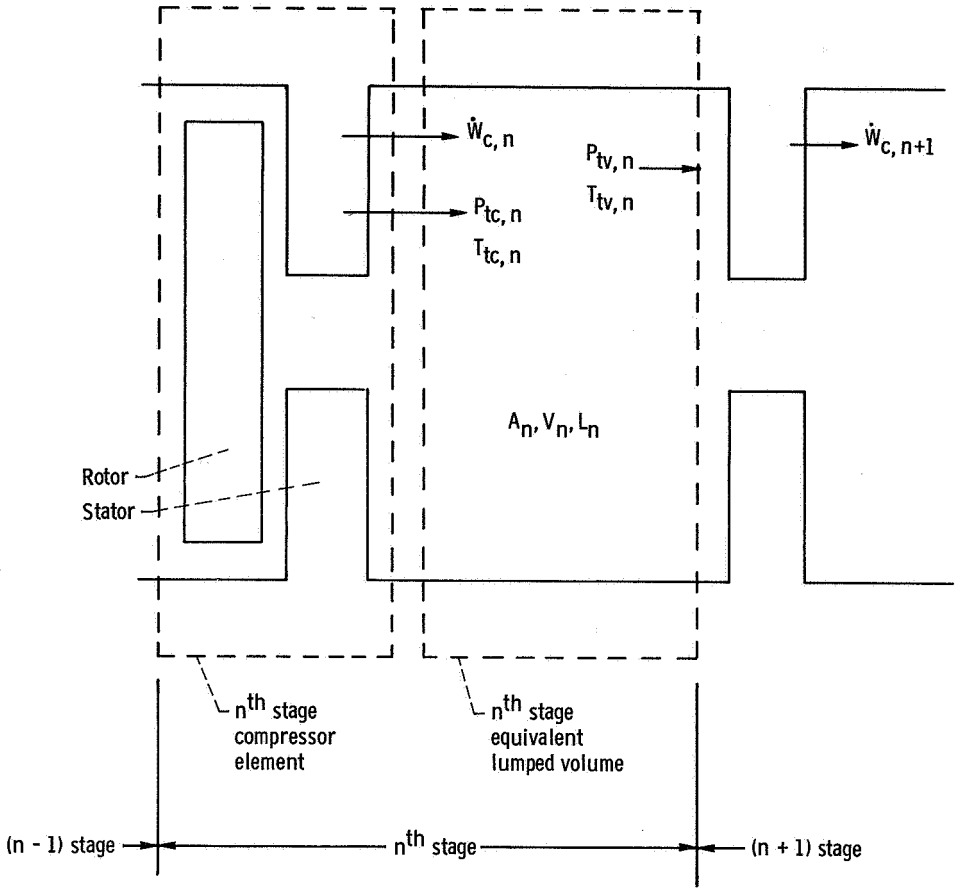

Figure 1. - Schematic of n^{th} stage compressor.

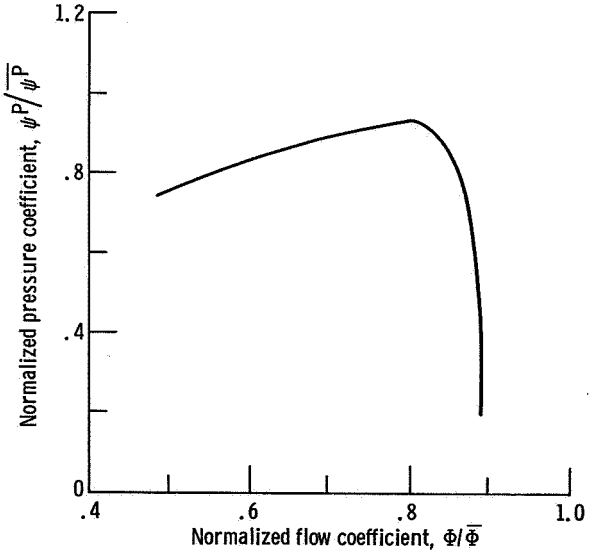

Figure 2. - Representative compressor stage pressure map.

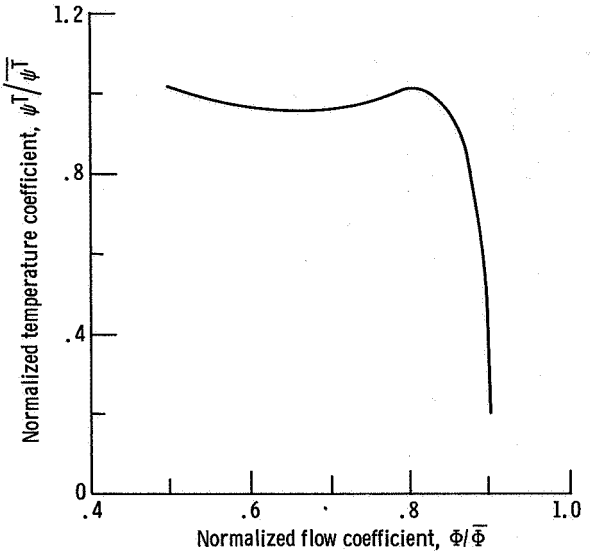

Figure 3. - Representative compressor stage temperature map.

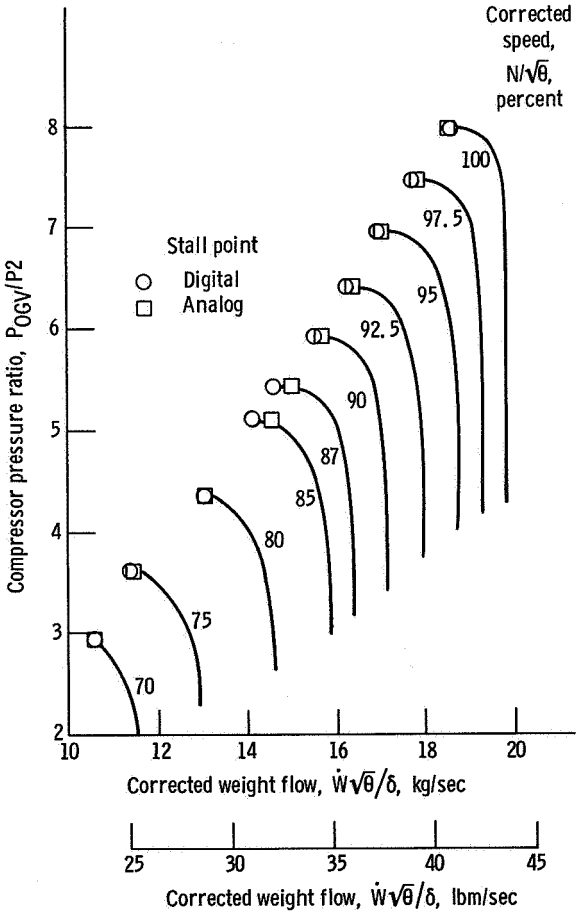

Figure 4. - Comparison of stall points generated analytically by unmodified analog and digital compressor simulations. Sea level static conditions.

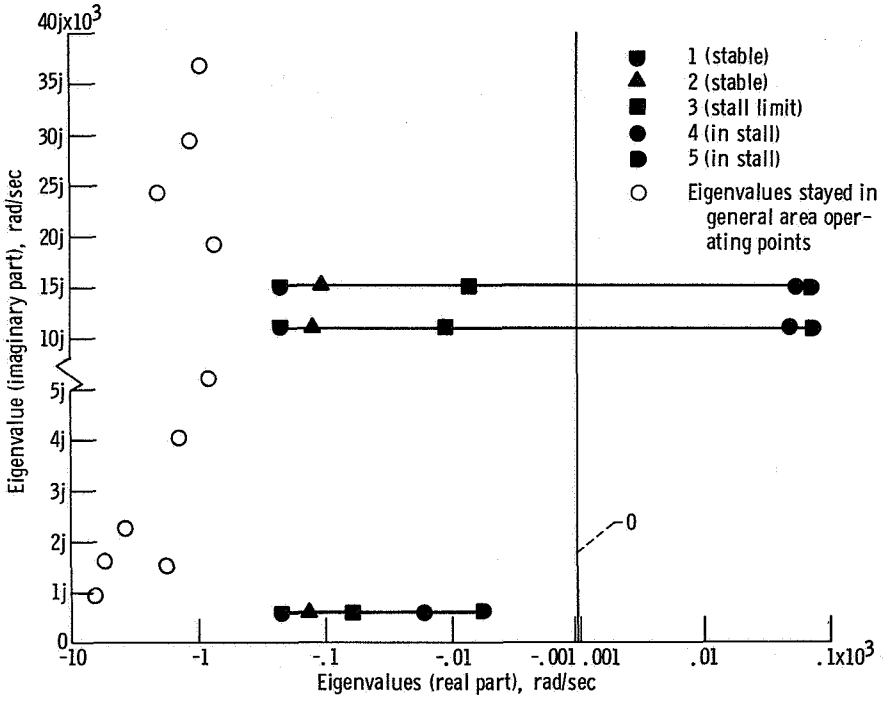

Figure 5. - Movement of eigenvalues as operating point moved slowly up 100-percent speed line. (26-State variable model.)

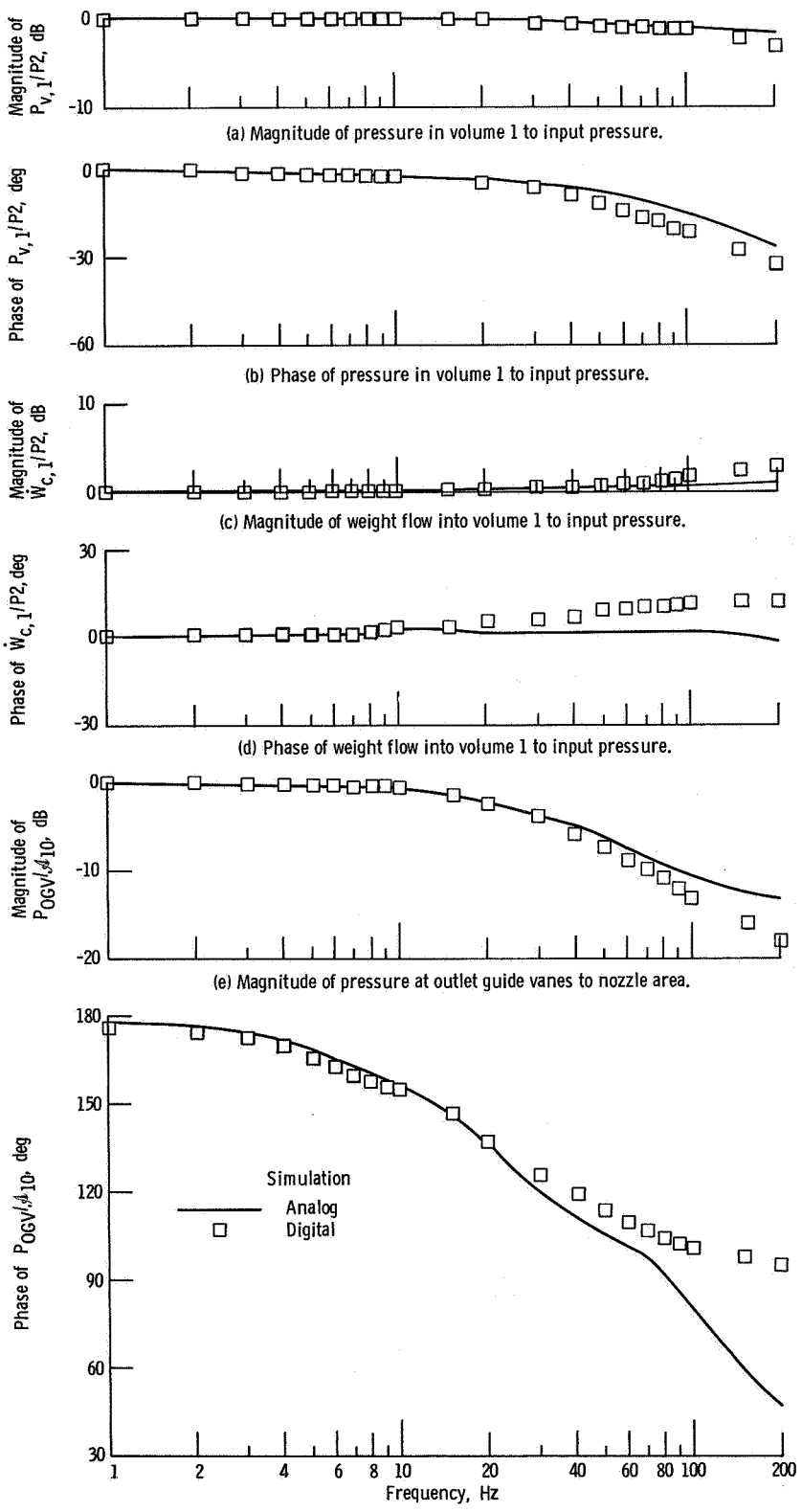

(a) Magnitude of pressure in volume 1 to input pressure.

(b) Phase of pressure in volume 1 to input pressure.

(c) Magnitude of weight flow into volume 1 to input pressure.

(d) Phase of weight flow into volume 1 to input pressure.

(e) Magnitude of pressure at outlet guide vanes to nozzle area.

(f) Phase of pressure at outlet guide vanes to nozzle area.

Figure 6. - Comparison of frequency responses generated by analog and digital J85 simulations.

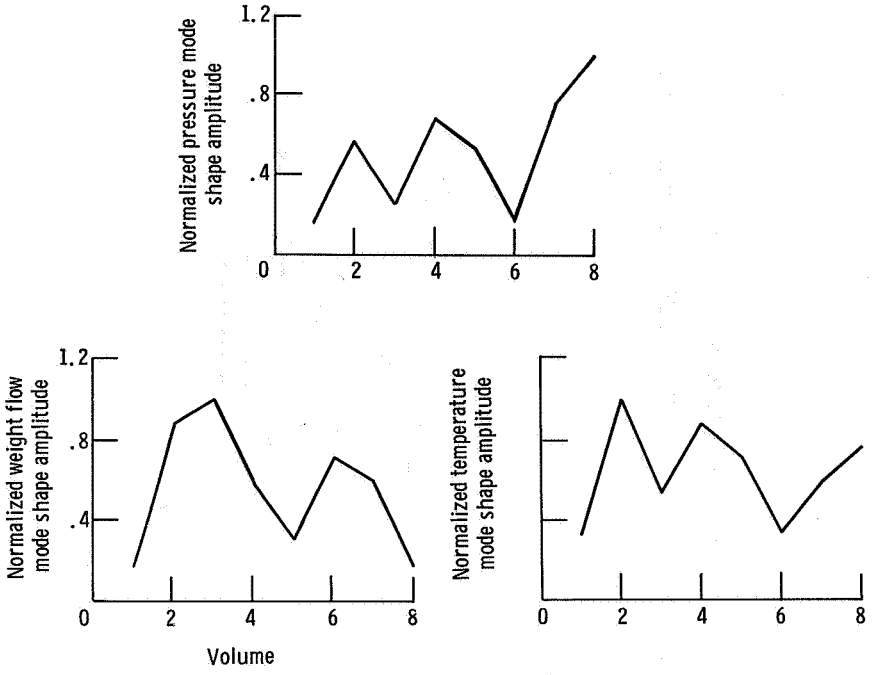

Figure 7. - Normalized pressure, weight flow, and temperature mode shape amplitudes associated with unstable eigenvalues on 100-percent speed line.

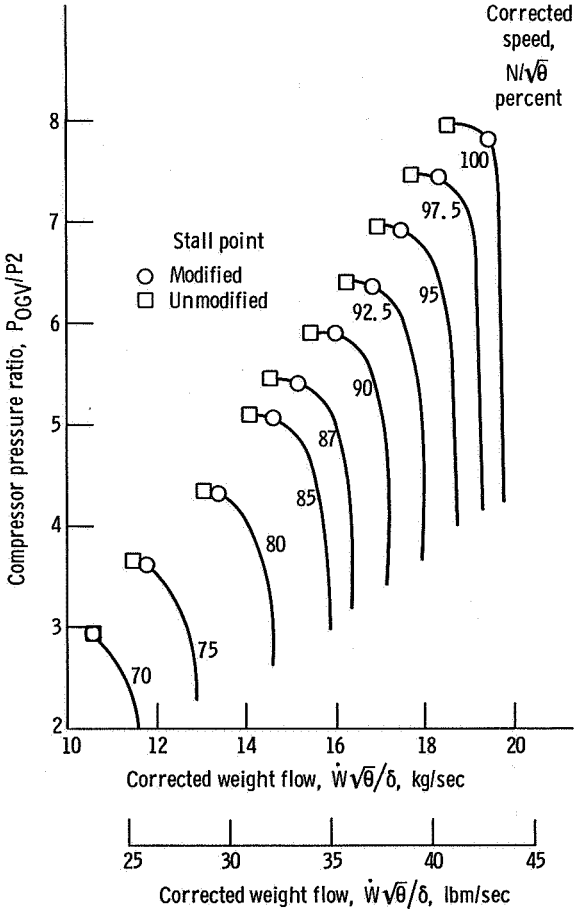

Figure 8. - Comparison of stall points generated analytically by unmodified and modified digital compressor simulations. Sea level static conditions.

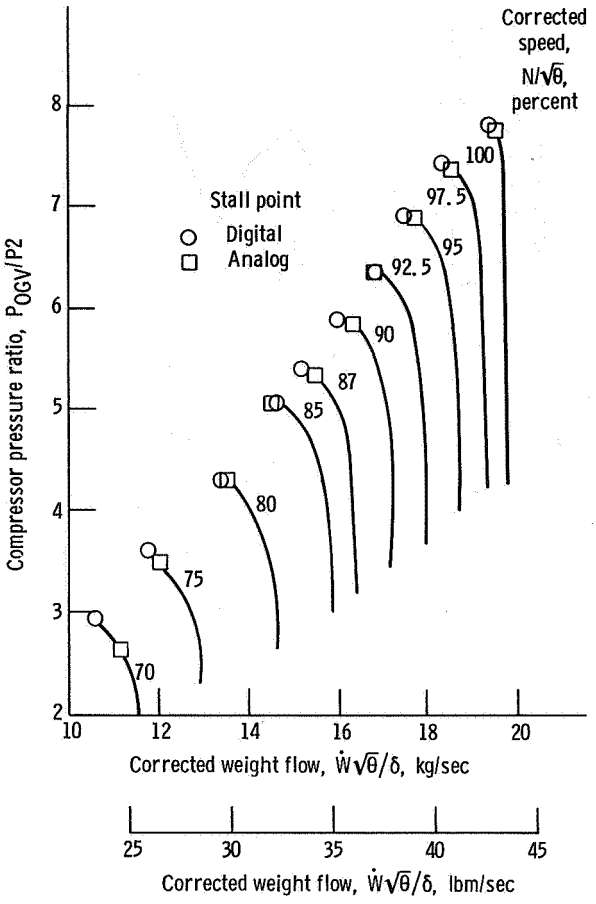

Figure 9. - Comparison of stall points generated analytically by modified analog and digital compressor simulations. Sea level static conditions.

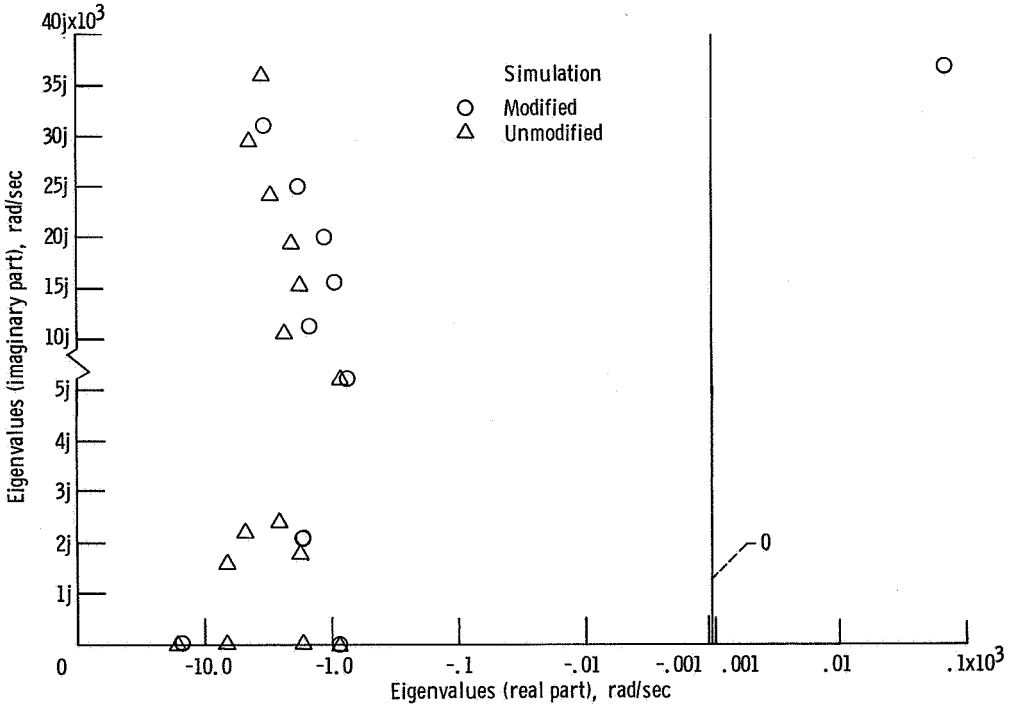

Figure 10. - Comparison of eigenvalues for modified and unmodified compressor digital simulations at point just after stall limit for modified compressor simulation.